Faraday Discussions

Accepted Manuscript

This manuscript will be presented and discussed at a forthcoming Faraday Discussion meeting. All delegates can contribute to the discussion which will be included in the final volume.

Register now to attend! Full details of all upcoming meetings: http://rsc.li/fd-upcoming-meetings

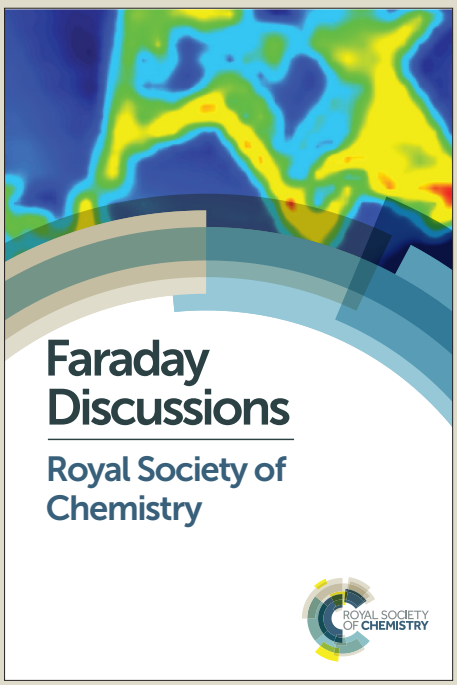

This is an *Accepted Manuscript*, which has been through the Royal Society of Chemistry peer review process and has been accepted for publication.

Accepted Manuscripts are published online shortly after acceptance, before technical editing, formatting and proof reading. Using this free service, authors can make their results available to the community, in citable form, before we publish the edited article. We will replace this *Accepted Manuscript* with the edited and formatted *Advance Article* as soon as it is available.

You can find more information about *Accepted Manuscripts* in the Information for Authors.

Please note that technical editing may introduce minor changes to the text and/or graphics, which may alter content. The journal's standard Terms & Conditions and the Ethical guidelines still apply. In no event shall the Royal Society of Chemistry be held responsible for any errors or omissions in this *Accepted Manuscript* or any consequences arising from the use of any information it contains.

ROYAL SOCIETY OF CHEMISTRY

www.rsc.org/faraday_d

Faraday Discussions

ARTICLE

Electrocatalytic conversion of CO_2 to produce solar fuels in electrolyte or electrolyte-less configurations of PEC cells

Received 00th January 20xx,
Accepted 00th January 20xx

DOI: 10.1039/x0xx00000x

www.rsc.org/

C. Ampelli,[a] C. Genovese,[a] B. C. Marepally,[a] G. Papanikolaou,[a] S. Perathoner,[a] and G. Centi,[a]

The electrocatalytic reduction of CO_2 is studied on a series of electrodes (based on Cu, Co, Fe and Pt metal nanoparticles deposited on carbon nanotubes or carbon black and then placed at the interface between a Nafion membrane and a gas-diffusion-layer electrode) on two types of cells: one operating in the presence of a liquid bulk electrolyte and the other in the absence of the electrolyte (electrolyte-less conditions). The results evidence how the latter conditions allow about one order of magnitude higher productivity and to change in the type of products formed. Under electrolyte-less conditions, the formation of >C2 products such as acetone and isopropanol is observed, but not in liquid-phase cell operations on the same electrodes. The relative order of productivity in CO_2 electrocatalytic reduction in the series of electrodes investigated is also different between the two type cells. The implication of these results in terms of possible differences in the reaction mechanism are commented, as well as in terms of design of photoelectrocatalytic (PEC) solar cells.

Introduction

A raising interest is present in literature on solar fuels [1-10], although different concepts are often associated to this definition. Solar fuels are indicated here those having a carbon-negative footprint, because they utilize the emitted CO_2 to produce energy carriers or chemicals through the use of renewable energy (RE) sources. The net effect is thus of introducing RE in the energy or chemical production cycle. The type of products obtained in this process is relevant, because they should be preferably *drop-in* liquid-fuels according to both economic and sustainability perspectives. In fact, it is often forgotten the many problems (economics, normative, authorization etc.) associated to the introduction of new products requiring a novel infrastructure. Being so large scale the problem of energy, a "sustainable" transition to a low-carbon economy is only possible by development of energy vectors and raw materials for chemistry, which smoothly integrate in the actual system and infrastructure, minimizing above issues. Liquid products are necessary to allow an energy-efficient and low cost transport to long distance and storage for long time, one of the actual main advantages of oil and derivate energy carriers.

We early discussed more in detail the above aspects, in relation to the need to develop a sustainable low-carbon energy and chemical production [11-14]. In this vision, CO_2, biomass and solar energy are the three key elements around which develop the future sustainable scenario for energy and chemical production [12,15]. Critical factors to enable this scenario are the development of new approaches for the electrochemical conversion of CO_2, a key step towards artificial leaf-type devices [7,16]. Many reviews have discussed recently the electrocatalytic conversion of CO_2 [17-23], as well as artificial leaf-type or photosynthetic devices [7,10,24-29], although only few of them may be cited.

The common aspect is the presence of a bulk electrolyte used to close the electric circuit in the electrocatalytic cell or photoelectro-catalytic (PEC) devices. We have shown, however, that a different approach is possible, indicated as electrolyte-less (EL), because a bulk liquid electrolyte is absent [30]. The ionic conduction is realized through a membrane having the photo- and electro-catalysts on the two opposite faces of the membrane, while the electronic conduction is realized through an external wire [31]. This EL approach allows to convert CO_2 electrocatalytically to >C1 products [32-34], while essentially C1 products, with traces C2 products are detected in the presence of an electrolyte [35-40].

EL design for PEC solar cells shows some advantages: (i) it is possible to operate at higher temperatures, allowing process intensification and the use of solar concentrators; (i) the problems related to CO_2 adsorption/diffusion in liquid phase are eliminated; (iii) the sealing and design of the cell is greatly simplified; (iv) gas-cap formation on the electrode (which may largely decrease the performances) is avoided; (v) operations under pressure are simplified; (vi) light scattering and absorption by the liquid are avoided; (vii) corrosion of the electrode (a main issue in conventional PEC cells) is virtually absent. However, the greatest advantage is the more effective (from the cost and energy perspectives) recovery of liquid products of CO_2 reduction, because they can be collected from

[a] Dept. DIECII, Section Industrial Chemistry,
University of Messina, CASPE/INSTM and ERIC aisbl.
V.le F. Stagno D'Alcontres 31
98166 Messina, Italy
e-mail: centi@unime.it

the gas stream leaving the EL-PEC cell and not from the liquid electrolyte, requiring distillation or other costly separation procedures. However, the electrodes in EL-PEC cell, or the hemi-cell for the electrocatalytic reduction of CO_2, should be different from the conventional ones utilized in PEC or electrochemical cells. In fact, together with good electron conductivity, the electrode for the electroreduction of CO_2 should guarantee a good transport of the protons coming from the membrane to the active centers for CO_2 reduction.

There is thus an intriguing question whether this difference in electrode characteristics is responsible for the different type of products observed experimentally during the electrocatalytic reduction of CO_2 or instead there are intrinsic differences in terms of reactivity and reaction mechanism deriving from the presence or not of a bulk liquid electrolyte. The electric double layer, which determines the characteristics of the interface at the catalytic centers, depends on the electrolyte. In PEC cells, concentrated electrolyte solutions are used to minimize internal resistance, but in EL-PEC cell approach the electrolyte is virtually absent. However, a thin liquid film may be present over the electrocatalysts. Although the ionic transport (to close the circuit) can be realized by surface transport over the electrocatalysts and then through the membrane (without thus the need of a liquid film over the electrode), a surface aqueous acid thin layer may eventually be present as well as capillary condensation in micropores may occur, depending on the temperature and pressure of operations. Nevertheless, the interface between the electrocatalysts and a bulk electrolyte is clearly different from that when the electrocatalysts is in contact directly with gas phase (CO_2), even when a thin aqueous film may be present. The concentration of CO_2 at the surface of the electrocatalyst is thus expected to be different. However, the different type of electrodes used in conventional and EL hemi-cells for the electrocatalytic reduction of CO_2 do not allow clarifying above question and obtain better insights on the motivations for the different behaviour between conventional and EL-cells in the electrocatalytic conversion of CO_2.

The aim of this contribution is thus to utilize the same type of electrodes and reaction conditions, except for the presence of the liquid bulk electrolyte, in order to compare conventional and EL approaches, determine more precise the differences in the productivity and type of products, and obtain indications about possible differences in the reaction mechanism.

Electrochemical cells for the reduction of CO_2

In electrochemistry, attention is typically focused on the electrode and operative conditions, while the cell design is often not considered, except in engineering terms of realization of an optimal charge transport, homogeneous flow and electron distribution in large cells, etc. The possibility to operate without a liquid electrolyte is not typically considered for the electrocatalytic reduction of CO_2, although PEM (Proton Exchange Membrane) fuel cells may be considered an example of EL operations. We will compare here two different approaches for the electrochemical reduction of CO_2: 1) gas phase (EL-cell approach) and 2) liquid phase, e.g. conventional

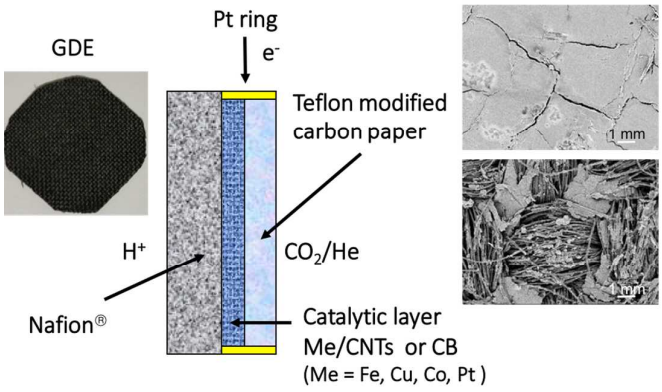

Figure 1: Schematic illustration of the GDE-type electrodes utilized for the CO_2 electrochemical reduction. Image on the left shows the full gas-diffusion electrode (GDE), while images on the right are scanning electron microscopy images of the side at contact with the membrane and of the side at contact with gas phase (CO_2) or the electrolyte in which CO_2 is bubbled.

one, although using the same type of electrocatalysts of the gas-phase approach. The two devices show common aspects:

i) the two electrodic compartments are separated by a proton selective membrane, which allows the migration of protons from the anode to the cathode side;
ii) the electrocatalyst (metal nanoparticles supported over a functionalized carbon nanotube - CNT) is located at the cathode side, supported over a conductive net (carbon paper) and in close contact with the membrane, while the external part at contact with the gas or liquid phase is coated with Teflon to realize a gas diffusion electrode (GDE) (Fig. 1) as in PEM fuel cells;
iii) CO_2 continuously flows to the cathode of the electrocatalytic cell as 100% CO_2 at a rate of 10-20 ml/min;
iv) the currents/potentials applied are similar (1-2 V; 10-100 mA).

These cells are the CO_2 reduction hemi-cells of PEC solar cells, where a photo-anode is also present. The latter is a photo-active material able to absorb sunlight to create a charge-separation, with the holes utilized at suitable catalytic centers for the reaction of water oxidation to produce O_2 and protons, the latter being transported to the electrocatalyst through the membrane. The electrons are instead collected and transported externally (through a wire) to the conductive electrocatalyst. We have studied the photo-anode behaviour by preparing TiO_2 nanostructured electrodes [33], doped with noble (Pt, Au) [41] and non-noble nanoparticles (Cu) [42] to enhance their visible response. Electrolyte and EL operations for the photo-anode side (indicated as liquid and gas phase operations, respectively) were both investigated. In water photo-electrolysis and ethanol dehydrogenation processes, higher performances (in terms of H_2 production) of the gas phase with respect to liquid-phase configuration were observed [42,43]. Therefore, a full EL-PEC cell may be developed, both for the anodic and cathodic parts. However,

discussion will be focused here only on the electrocatalytic reduction of CO_2, thus on the cathodic part of the PEC cell.

Experimental

Synthesis of the electrode materials

The working electrode for the electrochemical cells for CO_2 reduction consists of a carbon substrate on which the metal nanoparticles are deposited. This electrocatalyst is then deposited on a gas diffusion layer (GDL 25 BC Sigracet®), on the side not modified with Teflon. The carbon substrates are commercial Carbon Black (CB, Vulcan® XC-72) and Carbon Nanotubes (CNTs, PR-24-XT-PS Pyrograf®).

PR-24-XT-PS CNTs have an average diameter of about 100 nanometers. The inner part shows well-ordered graphitic layers aligned along the main axis, but the external surface displays a turbographic structure. The CNTs were pyrolyzed at 750°C to remove polyaromatic hydrocarbons from their surface. Due to the turbographic structure, these CNTs offer a large amount of sites for functionalization of the external surface.

The nature of the functional groups on the carbon surface plays a key role in the catalytic activity of the electrocatalysts. Thus, CNTs were functionalized by direct oxidative treatment in concentrated HNO_3, introducing oxygen functionalities on the carbon surface. In detail, 1 g of CNTs (or CB) was suspended in 50 mL HNO_3 (65 % Sigma Aldrich) and treated in reflux at 100°C for 3 h, followed by rinsing until neutral pH, filtering, and drying overnight. Different types of oxygen functionalities were introduced by this treatment. The total quantity and relative distribution can vary as a function of the annealing post-treatment in inert atmosphere, as shown from synchrotron radiation XPS data [23].

The main properties of commercial GDL and CNTs are reported in Table 1.

Table 1: Properties of the as-produced commercial materials used to prepare the electrocatalyst.

Properties of GDL 25 BC Sigracet®	
thickness	235 μm
areal weight	86 g/m^2
porosity	80 %
air permeability	1.0 cm^3/(cm^2 s)
electrical resistance (through plane)	<12 mΩ cm^2

Properties of CNTs PR-24-XT-PS Pyrograf®	
Fiber diameter (average)	100 nm
Surface area	45 m^2/g
Dispersive surface energy	85 mJ/m^2:
Moisture	<5 wt.%
Iron	<14,000 ppm
Polyaromatic hydrocarbons	<1 mg PAH/g fiber

Before depositing the carbon substrates on the GDL, metal (M = Cu, Co, Fe or Pt) nanoparticles (NPs) were deposited on CB and CNTs by incipient wetness impregnation method using an ethanolic solution containing the proper metal precursor [$Cu(NO_3)_2{\cdot}3H_2O$; $Co(NO_3)_2{\cdot}6H_2O$; $Fe(NO_3)_3{\cdot}9H_2O$; $H_2PtCl_6{\cdot}xH_2O$]. After drying at 60°C for 24 h, the samples were reduced for 2h at 350°C under a slow H_2 flow. The total amount of metal loaded onto the carbon substrate was 10 wt.%. This amount was chosen in order to have an amount comparable to the metal loading in the electrocatalysts for PEM fuel cells (usually 10-20 wt.%), which corresponds to a small metal loading in the final catalyst (about 0.5 mg/cm^2).

The as-prepared carbon substrates with the deposited nanoparticles were then deposited on GDL using a similar impregnation in anhydrous ethanol and after joining the GDL with the Nafion membrane, the samples were tested as working electrodes both in liquid and gas phase cell configurations. While in the liquid-phase cell the electrode is in contact with the electrolyte solution saturated with CO_2, in the gas-phase cell the electrode is absent and ionic conductivity is guarantee from the contact with the proton-conducting membrane (Nafion®). Before the use, the Nafion® membrane was pre-treated with hydrogen peroxide to eliminate organic impurities and finally activated with H_2SO_4.

Characterization

Surface area of the samples (BET method) was determined by the physical adsorption of N_2 at liquid nitrogen temperatures by using a Micrometrics ASAP 2010 system.

Transmission electron microscopy (TEM) images were acquired by using a Philips CM12 microscope (resolution 0.2 nm) with an accelerating voltage of 120 kV, while SEM images were recorded with a Philips XL-30-FEG scanning electron microscope.

Liquid-phase cell

The electrochemical cell, made in Plexiglas to allow visual inspection, has a three-electrode configuration and is schematically illustrated in Figure 2. The working electrode (about 3 cm^2) is located at the cathode side, at a small distance (0.5 cm) from a saturated Ag/AgCl electrode (working as reference electrode) to reduce the solution resistance. The electric contact with the working electrode is maintained with a Pt wire. The counter-electrode is a commercial Pt rod (Amel) immersed in the anode compartment. A potentiostat/ galvanostat (Amel mod. 2049A) is employed to supply a constant current/bias between the electrodes.

The anode compartment is physically separated from the cathode side by a proton-conducting membrane (Nafion® 117, Ion Power). A 0.5 M aqueous solution of $KHCO_3$ was used as electrolyte solution both in cathode and anode compartments. The volume of the electrolyte solution at the anode was about 9-10 ml. The electrochemical cell was designed in order to have a large surface area of the electrode and to minimize the electrolyte solution at direct contact with the electrocatalyst. A continuous flow of pure CO_2 (10 ml/min) was introduced into an external reservoir to saturate the electrolyte solution. This allows preventing interference from gas bubbles striking the

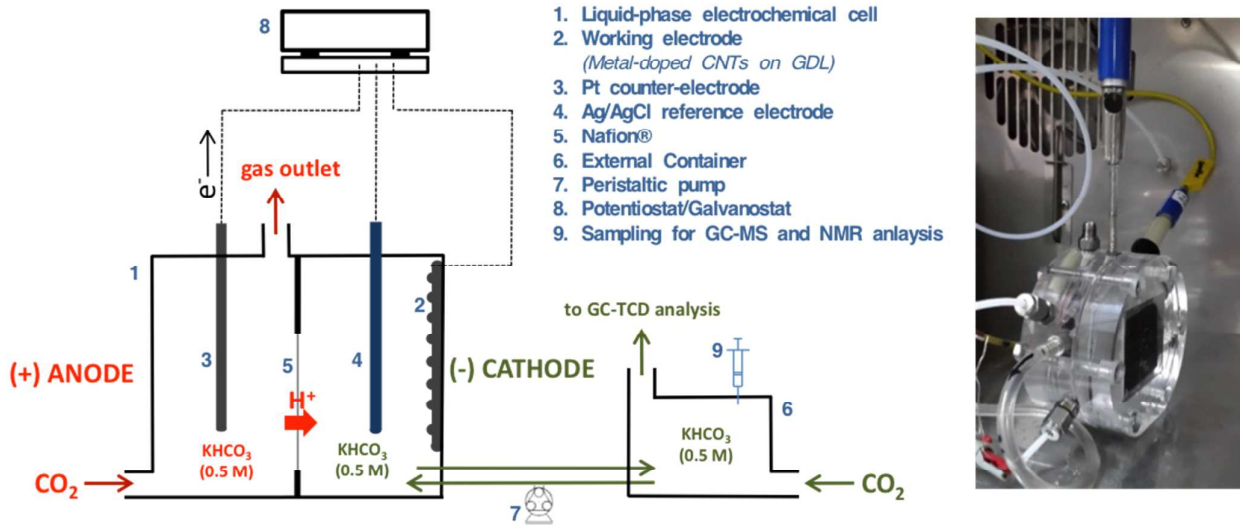

Figure 2: Schematic drawing of the experimental apparatus for electrocatalytic tests of CO_2 reduction in liquid phase, e.g. in the presence of a liquid electrolyte.

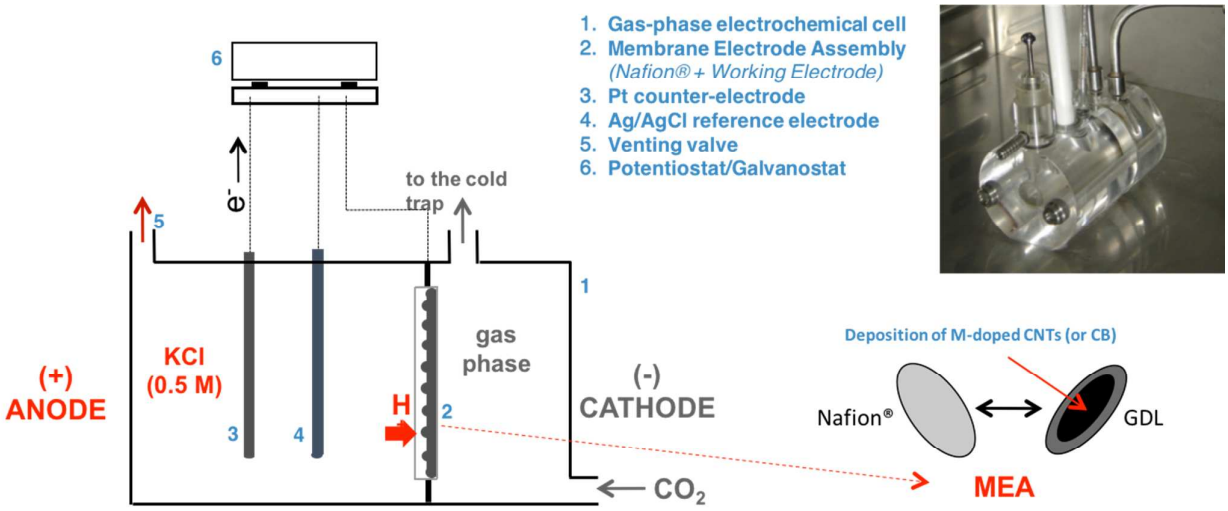

Figure 3: Schematic drawing of the experimental apparatus for electrocatalytic tests of CO_2 reduction in gas phase, e.g. in electrolyte-less (EL) conditions.

electrode surface in the cathode compartment. The electrolyte solution is continuously circulated between the cathode compartment and the external container by using a peristaltic pump. The total amount of solution (cathode + external container) was 20 ml.

The liquid products were analysed by sampling the liquid in the external container and determining the composition of the solution by ^{1}H Nuclear Magnetic Resonance Spectroscopy (NMR, Varian NMR 500) and by Gas Chromatography-Mass Spectrometer (GC-MS, Thermo Trace 1310, ISQ SIngle Quadrupole MS, column Stabilwax MS). The gas products were detected by sampling the gaseous stream leaving the external container at regular intervals and analysing by Gas-chromatography (GC- TCD, Agilent 7890A, column 5A Plot).

Gas-phase cell (EL conditions)

The electrochemical cell for CO_2 reduction working in gas-phase (electrolyte-less – EL – conditions) was designed to operate under a continuous flow of CO_2 diffusing through the GDL to arrive to the surface of the electrocatalyst. The cell was made in Plexiglas and it is located within an oven to work eventually at higher temperatures, up to about 70-80°C, although all the tests reported here were carried out at room temperature to be comparable to those in the liquid cell, which do not allow operations at temperature above about 40°C. Figure 3 reports a schematic drawing of the experimental apparatus.

The cell has a three-electrode configuration, with a Pt wire as counter-electrode and a saturated Ag/AgCl electrode as

reference electrode, both immersed in the anode compartment. A Membrane Electrode Assembly (MEA) separates the two cell compartments. The MEA consists of: i) a proton-conducting membrane (Nafion® 117) and ii) the electrocatalyst deposited on the GDL. These two samples were assembled together by hot pressing at 80 atm and 130°C for 90s. The electrocatalyst is located at the interface with the membrane. The anode side, to be more comparable with the liquid cell, works in liquid phase and it used to provide the protons (through the Nafion membrane) needed for the CO_2 reduction process. The anode side is filled with an electrolyte aqueous solution (KCl 0.5 M) and it is in direct contact with one side of the Nafion® membrane. A gas flow of pure CO_2 (10 ml/min) is continuously fluxed into the cathodic compartment.

A potentiostat/galvanostat (Amel mod. 2049A) was used to supply a constant current (10-20 mA) between the electrodes. The voltage increases as a function of time-on-stream during the first hour stabilizing to a value of about around 1.4 to 1.5 V. At the end of the reaction (typically 1 h), the current polarity was inverted to facilitate desorption of the products from the working electrode. The liquid products were collected in a cold trap from the flux leaving the cathodic part of the cell. They are analyzed by a gas chromatograph equipped with a mass detector (Thermo Scientific GC Trace 1310 – ISQ MS).

Table 2: Characterization of the textural characteristics of the electrocatalysts by BET method.

Electro-catalyst	a_{BET}, $m^2 \cdot g^{-1}$	V_m, $cm^3 \cdot g^{-1}$	*Average pore diameter, nm*
CNT_{ox}	23,1	5,3	11,4
Cu-CNT_{ox}	48,3	11,1	10,8
Co-CNT_{ox}	72,6	16,7	14,9
Fe-CNT_{ox}	63,8	14,6	9,2
Fe-CB	221,2	50,8	12,2
Pt-CNT_{ox}	23,6	5,4	11,3

Results and Discussion

Characterization of the electrodes

The BET characterization of the electrocatalysts is reported in Table 2. An increase in the surface area and pore volume after the addition of Cu, Co, Fe nanoparticles is observed, but not for Pt, although no relevant changes in the average pore volume were observed in all cases. The effect may thus be interpreted as a reduced sticking between the CNTs, due to the change in the surface properties of functionalized CNTs during the process of addition of the metallic nanoparticles. On the contrary, the samples based on CB (carbon black) as support (only iron sample is reported in table 2, being the results for the other samples quite similar) have significantly larger BET surface area and pore volume.

Figure 4 reports an image by TEM of Fe-CNT sample. It may be observed the presence of a good dispersion of iron particles, preferentially located on the external surface of CNT. The average size is between 3 and 5 nm, with relatively narrow distribution. A similar well distribution of the metal nanoparticles is observed in the other samples. Pt allows obtaining slightly lower average size for the metal particles, centred around 1-3 nm. A good dispersion is also observed in the samples based on CB support, without determining relevant differences in terms of dispersion and average metal nanoparticle size. It may thus be concluded that in spite of the different surface area, both CNT_{ox} and CB allow to obtain a good dispersion of the metal nanoparticles and analogous average size of them.

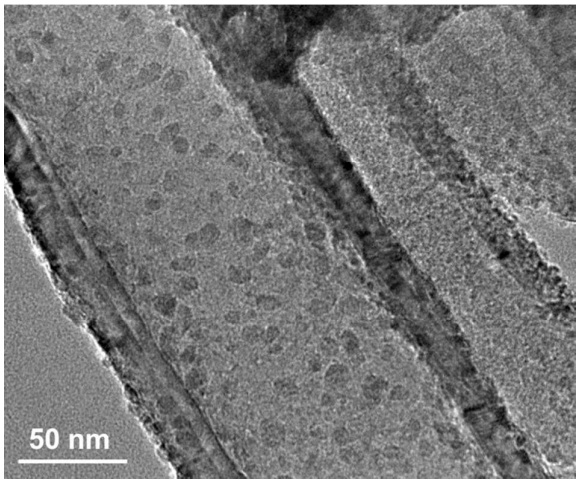

Figure 4: Transmission electron microscopy (TEM) image of Fe-CNT sample.

CO_2 electrocatalytic reduction in liquid phase cell

The main products detected in the liquid electrolyte in the cathode side are reported in Table 3 for all the electrocatalysts tested in liquid-phase cell. As reference, (i) metal Cu foil and (ii) CNT_{ox} alone (e.g. without metal particles, but deposed on GDL) were analysed.

Table 3: Main products formed in 1h of reaction in the CO_2 electrochemical reduction in liquid phase.

Electrode	*Formic acid [M]*	*Acetic acid [M]*	*Methyl formate [M]*
Cu foil	6.1e-4	4.0e-4	-
Cu-CB/GDL	3.6e-5	1.4e-5	1.7e-4
Fe-CB/GDL	4.6e-5	5.4e-5	6.0e-6
Co-CB/GDL	8.1e-5	9.5e-5	7e-6
Cu-CNT_{ox}/GDL	1.2e-4	8.4e-5	1.5e-5
Fe-CNT_{ox}/GDL	1.8e-5	2.1e-5	1.2e-5
Pt-CNT_{ox}/GDL	2.3e-4	1.8e-4	-
CNT_{ox}/GDL	2.2e-5	1.4e-5	-

The main products detected in the liquid electrolyte solution were: formic acid, acetic acid and methyl formate. Pure Cu foil electrode forms also methanol in traces. The main other product of reaction, detected in the gas stream leaving the cell (see Fig. 2) is H_2, while CO, CH_4 or C2 hydrocarbons were not detected in all the samples.

The first interesting observation is that CNT_{ox} itself is able to form H_2 (from protons and electrons), as well as some products of CO_2 conversion. In the absence of CNT, the products of CO_2 conversion were instead not detected. Thus, CNT itself (without metal particles) is able to convert electrocatalytically CO_2. It is worth to note that without the oxidative pretreatment, the CNT results inactive, thus the behaviour observed cannot be attributed to residual traces of metal utilized for the synthesis of CNT itself (by catalytic chemical vapour deposition). The activity has to be related to the oxygen functional groups created during the CNT pretreatment (see experimental part).

Formic acid formation may be explained as deriving from the reaction of H_2 (formed by the catalytic electroreduction of the protons diffusing through the membrane) with the CO_2 present in the electrolyte. However, bubbling together H_2 and CO_2 in the absence of potential/current applied to the electrode do not result in the formation of products of CO_2 conversion. Reasonably, the functional groups present on CNT_{ox}, likely chetonic groups as observed for other catalytic reactions [44], are able to reduce CO_2 to formic acid according to a mechanism tentatively outlined in Scheme 1.

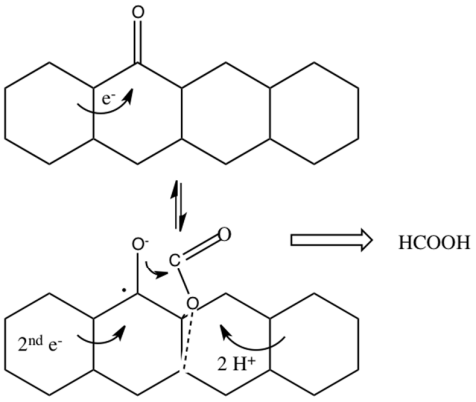

Scheme 1: Tentative reaction mechanism of CO_2 at chetonic groups present on the surface of CNT_{ox}.

Chetonic groups present at the edges or defects of CNTs may act as trapping sites for electrons, forming resonance species as outline in Scheme 1. The presence of an electron localized on the carbon activates the nearlying C-C bond, becoming able to coordinate the oxygen in CO_2, breaking also the molecule from linearity. The activation of nearlying C-C bonds, making susceptible for O_2 activation, is the mechanism proposed for N-doped CNTs active in oxygen reduction reaction (ORR) [44,45].

Acetic acid is the other main product observed using CNT_{ox}/GDL electrocatalyst (Table 3). It is not easy to explain the formation of this product. A preliminary hypothesis is that the further reduction of formic acid, with a mechanism similar to that outlined in Scheme 1, leads to the formation of formaldehyde. Formaldehyde may selectively transform with even 100% selectivity to acetic acid in relatively mild conditions (100°C, 500 psi CO) in the presence of a strong acid (HI) [46]. Formic acid in strong acid conditions (as present near the electrocatalyst surface, being located close to the Nafion membrane) decomposes to CO and H_2O. Carbon monoxide may react with formaldehyde in the presence of strong acid to selectively give acetic acid (a variation of Kock-Haaf reaction) [46]. It is reasonable that a similar mechanism occurs in our case during the electrochemical reduction of CO_2:

$$CO_2 - (2e^-, 2H^+) \rightarrow HCOOH \quad (1)$$

$$HCOOH - (\text{strong acid catal.}) \rightarrow CO + H_2 \quad (2a)$$

$$HCOOH - (2e^-, 2H^+) \rightarrow HCHO + H_2O \quad (2b)$$

$$HCHO + CO - (\text{strong acid}, H^+) \rightarrow CH_3COOH \quad (3)$$

This may also account why methanol, the further product of formaldehyde reduction, is not observed.

The presence of a metal nanoparticle leads to an increase in the productivity in the conversion of CO_2 and the presence of methyl formate in some cases (Table 3). The latter reasonably derives from the reaction of formic acid esterification with methanol under acid conditions:

$$HCOOH + CH_3OH - (\text{strong acid}) \rightarrow HCOOCH_3 + H_2O \quad (4)$$

Methyl formate may thus be associated with the formation of methanol and its fast conversion under the reaction conditions present in our experiments.

Various other observations can be made on the results evidenced in Table 3. Copper-based electrodes have been tested in three types of forms: as Cu foil (as reference, being one of the type of electrodes often utilized in the electrocatalytic reduction of CO_2), and in the form of copper nanoparticles supported over CNT_{ox} or CB. It may be observed that methyl formate is observed in both cases using CB or CNT_{ox} as support for copper nanoparticles, but not when copper foil is used. This result indicates that the presence of copper metal nanoparticles supported on carbon materials rather than copper itself (as suggested often in literature) promotes the formation of methanol. In terms of productivity, Cu-CB/GDL has nearly one order of magnitude higher formation of methyl formate than Cu-CNT_{ox}/GDL, although the copper amount and size of the copper nanoparticles is analogous. The higher surface area of CB with respect to CNT_{ox} (Table 2) may thus be not the reason for the different behaviour, being dispersion of copper in the two supports relatively similar. We may also note in Table 3 that formic and acetic acid formation is instead higher in Cu-CNT_{ox}/GDL in comparison to Cu-CB/GDL. Thus the main difference between the two samples is in the rate of the further reduction of formaldehyde to methanol:

$$HCHO - (2e^-, 2H^+) \rightarrow CH_3OH \quad (5)$$

with methanol then further reacting according to eq. (4). CB (Vulcan XC-72) contains about 0.3% S, present as sulphonic groups (-SO_3H) on the surface. These acid groups, stronger than the –COOH groups present on CNT_{ox} as a consequence of the oxidative pretreatment, reasonably favour a better surface transport of protons coming from the membrane. Probably the difference in the behaviour observed between CNT_{ox}/GDL and Cu-CB/GDL is associated with the different concentration of protons at the electrocatalytic centers, although this hypothesis should be better proof. A higher proton concentration favours the further reduction up to methanol, reducing the rate of side reactions. In fact, Table 3 shows that productivity to acetic acid (which can be considered a side reaction with respect to methanol formation) is about sixth time higher in CNT_{ox}/GDL with respect to Cu-CB/GDL, which parallel the strong decrease in methyl formate productivity.

The comparison of the results of Cu-foil electrode wit those of Cu-CB/GDL and Cu-CNTox/GDL electrodes provides some further interesting indication. To estimate the amount of copper present in the two types of samples, it may be considered that in Cu-CB/GDL or Cu-CNT_{ox}/GDL the total amount of copper in the 3 cm^2 electrode is about 1.5 mg. To estimate the amount of copper active in copper foil, it is not possible to just have the weight of the foils, but may be assumed a foils of the same electrode size (3 cm^2), but having a 10 nm thickness to have a comparable thickness to the size of copper nanoparticles in the samples over carbon support.

Considering for copper a density of 8.9 g/cm^3, this estimated amount of "surface" copper in copper foil is about 0.03 mg, thus significantly lower than that present in the "3D-like" electrodes based on carbon support. Alternatively, it may be considered the surface area of metal copper. For copper-foil, it is simple the geometrical electrode area for copper foil, e.g. 3 cm^2. For copper nanoparticles, the surface area can be indicatively estimated assuming round-shaped copper nanoparticles of 10 nm size. With this simplification, the surface area for a total amount of 1.5 mg of copper in the electrode results to be about $0.5 \cdot 10^6$ cm^2, e.g. much largely than that of the geometrical surface of the copper foil electrode. It may be argued that the real surface of copper foil is not flat, but some roughness is present as well as some porosity. Also for metal nanoparticles, the part of the surface in contact with the carbon is not accessible (lowering the electrocatalytic active surface), but also smaller particles than 10 nm are present, increasing the overall metal surface. However, the differences estimated for the two types of electrodes (copper foil and copper nanoparticles on carbon support) are so large to indicate that the issue is not related to a too simple model to calculate the active surface area of copper.

Therefore, the electrocatalytic active copper is much lower in copper-foil than in samples supported over carbon. Nevertheless, the productivity in conversion of CO_2 is about five times higher in Cu-foil than that of Cu-CB/GDL sample and even more with respect to Cu-CNT_{ox}/GDL (Table 3). This

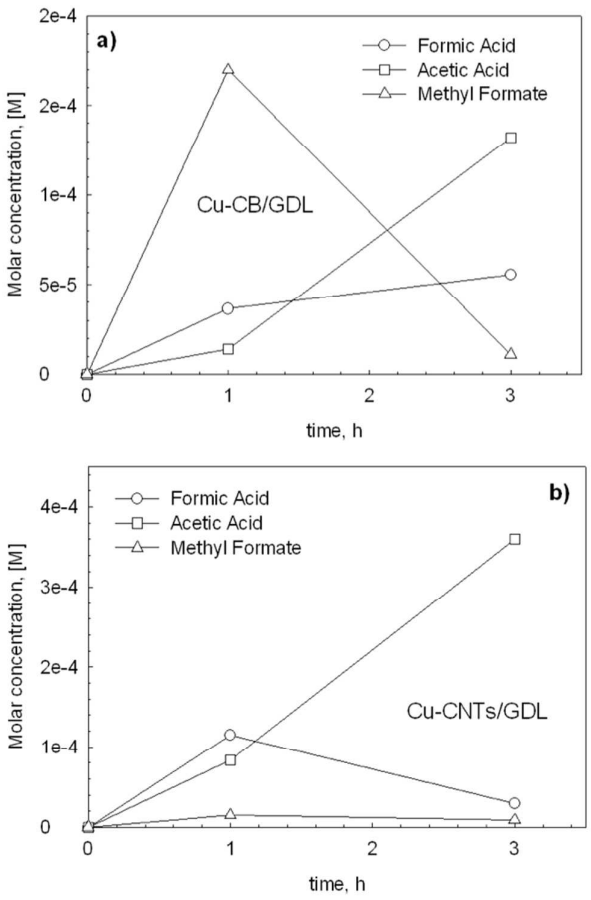

Figure 5: Time dependence of formic acid, acetic acid and methyl formate formation for liquid-phase testing experiments with a) Cu-CB/GDL and b) Cu-CNT_{ox}/GDL electrocatalysts.

indicates that transport of proton/electron as well as CO_2 diffusion to the active electrocatalytic centers is dominating the behaviour and productivity is not related to the metal active surface area in our experimental conditions.

This conclusion may also explain why notwithstanding some differences, the behaviour of other metal nanoparticles, namely iron and cobalt, is not significantly different from that observed for copper nanoparticles (Table 3). However, copper, particularly when on CB support, allows significantly higher methyl formate formation with respect to iron nanoparticles on the same support. Pt nanoparticles, on the contrary, do not form methyl formate but, as for Cu foil, they give larger quantities of formic acid as well as acetic acid.

The change of production rate with time during liquid-phase cell experiments is shown in Figure 5 for Cu-CB/GDL and Cu-CNTs/GDL electrodes. Formic acid formation decreases after 3h of reaction, while the concentration of acetic acid increases in both the cases in agreement with the reaction mechanism discussed before. The methyl formate concentration in liquid phase is higher after 1h for Cu-CB/GDL, strongly decreasing after 3h, due to its high volatility (methyl

formate boiling point = 32°C). Traces of methyl formate were found in the gas outlet from the external container.

It should also be commented that pH changes greatly influence the performances, in agreement with discussion on the possible reaction mechanism. The aqueous electrolyte used for liquid phase experiments is $KHCO_3$ (0.5 M). When CO_2 is bubbled into the hemi-cell compartments, an acid-base equilibrium between CO_2 and HCO_3^- establishes in solution:

$$CO_2 + H_2O \prod HCO_3^- + H^+ \quad (6)$$

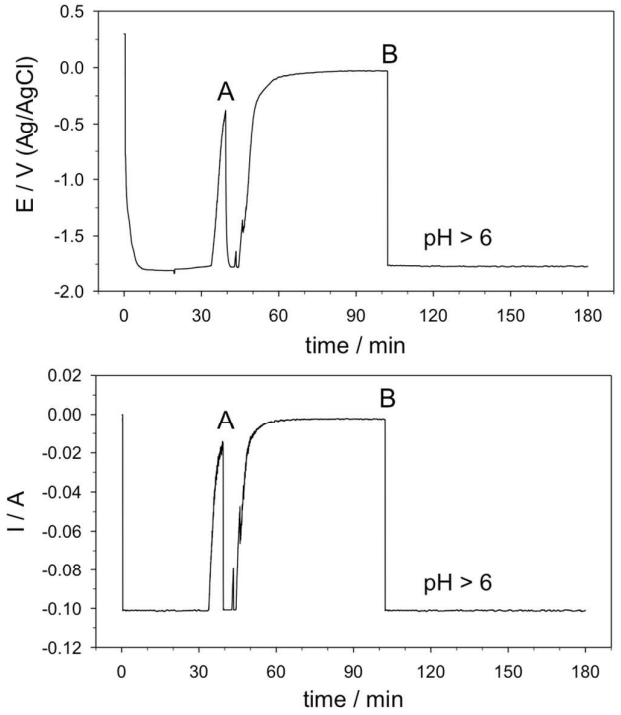

Figure 6: Profiles of voltage (E) and current (I) as a function of time in experiments in liquid-phase. (A) addition of some drops of fresh electrolyte solution (0.5 M KHCO3); (B) addition of some drops of 1 M NaOH aqueous solution to maintain pH in the anode part at pH > 6.

The pH of the fresh electrolyte is about 12, but decreases to about 9 when CO_2 is bubbled in it. A small flow of pure CO_2 (10 ml/min) was also fluxed directly into the anode compartment to favour desorption of O_2 and oxygen species on the Pt counter-electrode surface which may increase the overpotential of the cell [47]. The flux of CO_2 in both the compartments of the cell also avoids to create pH gradients related to solubilisation of CO_2, as indicated in eq. (6). However, the pH in the anodic section varies as a consequence of the reaction. The pH of the electrolyte solution at the anode compartment is initially 6. It maintains stable during the first 30-60 min, depending on the electrocatalyst in the cathodic part. During this initial time, the voltage and current given to the electrochemical cell maintain stable (Fig. 6). Then, a sharp decrease of both the current and potential is observed, due to the following reaction at the anode, which decreases the pH inhibiting the half-reaction at the anode:

$$H_2O \prod 1/2O_2 + 2H^+ + 2e^- \quad (7)$$

By adding some drops of 1 M NaOH aqueous solution, the pH increased to values above 6 and the current rapidly returned back to the set-point value. In order to have stable performances, it is thus necessary to maintain the pH at > 6 in the anodic part by adding a base.

This evidences that transport of protons across the membrane is the rate limiting process in our case, because otherwise they should be transported to cathodic part where are consumed to generate H_2 and reduce CO_2.

The comparison of these results with those reported in literature in terms of TOF (turnover frequency) is not easy, because the cell /electrodes and cell operation conditions are different and TOF values are typically not reported in literature for the electrocatalytic reduction of CO_2. Kuhl et al.[35] have not only made a quite detailed investigation of this reactions, but have also reported the TOF values for each of the products determined (in the supplementary part). Due to the different type of electrode (a copper foil mechanically polished) and reaction conditions, they observed different type of products in the reduction of CO_2 (CH_4, formate, CO, methanol, ethylene, ethanol, glycolaldehyde, acetaldehyde, acetate, ethylenglycol, n-propanol, allyl alcohol, acetone). It is thus possible to compare the total TOF in products of CO_2 reduction, rather than for the single species. The results are reported in Table 4. A potential of -1.1 V (vs. RHE), corresponding to the maximum formations of products of CO_2 reduction in the Kuhl et al.[35] results, was chosen for this comparison. TOF data are reported as $\mu mol \cdot s^{-1} \cdot cm^{-2}$, e.g. the same unit used by Kuhl et al.[35]. They reported in parallel also TOF values expressed as molecules·s^{-1}·surface Cu atoms^{-1}. However, this estimated requires a series of assumptions on the number of Cu atoms which are even less valid in our case, due to the different type of electrodes. Having Kuhl et al.[35] used only a Cu foil electrodes, we reported TOF data in Table 4 only for Cu-based electrode, for a more homogeneous comparison. TOF results may be easily derived for the other electrodes, being proportional to the total amount of products formed. Having not detected in our case CO formation, results of Kuhl et al.[35] are differentiated to include or not the amount of CO formed. However, difference are limited.

As shown in Table 4, TOF data in our electrodes are from three times higher (for dispersed Cu nanoparticles on carbon support) to 13 times higher (for Cu foil).

Table 4: TOF values ($\mu mol \cdot s^{-1} \cdot cm^{-2}$) on copper-based electrodes, in comparison with TOF values reported by Kuhl et al.[35] (*) for Cu foil electrode.

Electrode	*TOF (all products)*	*TOF (all products, except CO)*	*TOF (all products)*
Cu foil	9,35e-2	-	-
Cu-CB/GDL	2,04e-2	-	-
Cu-CNT$_{ox}$/GDL	2,03e-2	-	-
Cu foil (*)		6,66e-3	6,96e-3

CO_2 electrocatalytic reduction in gas phase cell (EL operations)

Experiments made in the gas-phase electrochemical cell on the same electrodes used for liquid-phase cell show relevant differences, regarding both the types of products formed and the productivity. However, a common aspect in both cells is the relevant formation of H_2. Hydrogen is an undesired product, because reduces the Faradaic efficiency to the products of CO_2 reduction. This indicates that in our experimental conditions the use of electrons/protons for the reduction of CO_2 is a slower process with respect their recombination to form H_2. Inhibiting the last reaction is thus a requirement to improve the performances in the electrocatalytic reduction of CO_2. On the other hand, these results also evidence that formation of H_2 is a facile reaction not specifically requiring dedicated catalysts.

There are main differences in the type of products of reaction between liquid- and gas-phase cell operations, e.g. presence or not of the bulk electrolyte. In the gas outlet stream leaving the cathodic part of the cell, together with H_2, CO and in small amount CH_4 are also detected in the case of EL operations. The two last products are not detected in liquid phase operations. Although CO may form from formic acid decomposition (eq. 2a) in liquid-phase operations, it immediately reacts and CO is not detected in the products stream leaving the cell, at least up to detection limit. On the contrary, CO is a main product of CO_2 electrocatalytic reduction in gas-phase cell operations, indicating a different mechanism of formation, with probably CO being the primary product of CO_2 reduction, rather than a secondary product, as observed in liquid-phase operations. This may explain why methane, deriving from the catalytic reduction of CO on copper, iron and cobalt metal nanoparticles, is observed even if in small amounts in experiments with gas-phase cell, but not in those with liquid-phase cell.

The type of liquid products formed, detected in the electrolyte or condensed in the cold trap from the gaseous stream leaving the gas-phase cell, are also different in the two cases. Table 5 summarize the behaviour of the different type of tested electrodes in gas-phase cell (EL conditions). A first observation is that different types of products are observed:

i) methanol, rather than formic acid as C1 main product (together with CO);
ii) acetaldehyde, ethanol together with acetic acid as C2 products, while only the latter was observed together with methyl formate in some electrocatalysts;
iii) acetone and isopropanol as C3 products, while no C3 products were detected in liquid phase operations.

This different type of products clearly suggests a different type of mechanism of CO_2 electrocatalytic conversion, in agreement with what commented before. Table 6 summarizers the difference observed in the type of products of reduction of CO_2 between gas-phase and liquid-phase cell operations.

Table 6: Comparison of types of products obtained in liquid and gas phase operations in CO_2 electrocatalytic reduction

Gas phase	Liquid phase
Methanol *Acetaldehyde* *Ethanol* *Acetone* *Isopropanol* *Hydrocarbons C4-C9 (in traces)*	*Formic acid* *Acetic acid* *Methanol (in traces)*

It may be evidenced that the productivity is also different between gas-phase (Table 5) and liquid-phase (Table 3) operations, but also the relative order of activity. In gas-phase cell, the best productivity to products of CO_2 reduction is shown by Fe-CNT_{ox}/GDL (around $4.8 \cdot 10^{-4}$ mmol/h). The same electrode in liquid phase operations, considering the total volume of electrolyte, has a productivity of about $0.3 \cdot 10^{-4}$ mmol/h, e.g about one order of magnitude lower. For Cu-CTN_{ox}/GDL catalyst, productivity in gas-phase operations is about $1.4 \cdot 10^{-4}$ mmol/h, while in liquid-phase operations about $0.15 \cdot 10^{-4}$ mmol/h. Thus again about one order of magnitude difference is observed.

Also the relative order of productivity to products of CO_2 reduction is different, being in gas-phase cell (Table 5):

Fe-CNT_{ox}/GDL > Fe-CB/GDL > Cu-CNT_{ox}/GDL >Pt-CNT_{ox}/GDL

while for liquid-phase cell (Table 3)

Pt-CNT_{ox}/GDL ≈ Fe-CNT_{ox}/GDL > Cu-CNT_{ox}/GDL > Fe-CB/GDL

This observation further remarks that different aspects may determine the productivity in the reduction of CO_2, reasonably associated to the different reaction mechanism.

Differences in the reaction mechanism

The clarification of above question requires a more in depth analysis of the reaction mechanisms, with operando techniques, which, however, are not simple to apply to electrochemical tests under relevant environmental conditions. We may thus advance only some initial considerations, which help in setting the scene for more detailed mechanistic studies.

Table 5: Products obtained in the CO_2 electrochemical reduction in gas-phase.

Electrode	*Methanol, mmol/h*	*Acetaldehyde, mmol/h*	*Ethanol, mmol/h*	*Acetone, mmol/h*	*Isopropanol, mmol/h*	*Acetic acid, mmol/h*	*H_2, mmol/h*	*CO, mmol/h*
Co-CNT_{ox}/GDL	1.2e-4	4.5e-5	2.0e-4	1.3e-6	-	3.4e-5	2.0e-1	3.2e-2
Cu-CNT_{ox}/GDL	4.8e-5	1.1e-5	6.7e-5	1.0e-7	9.3e-6	-	1.7e-1	9.6e-3
Fe-CB/GDL	1.1e-04	2.9e-5	1.1e-4	1.2e-6	1.1e-6	1.5e-5	3.2e-1	3.6e-2
Fe-CNT_{ox}/GDL	1.4e-4	6.7e-5	9.4e-5	1.8e-7	8.4e-5	9.2e-5	3.6e-1	6.5e-2
Pt-CNT_{ox}/GDL	1.0e-5	1.7e-5	3.6e-5	1.7e-7	2.4e-5	1.4e-5	4.5e-1	3.5e-2

As earlier commented, the mechanism in liquid-phase may be associated (on the specific carbon-based electrocatalysts we utilize) with the activation mechanism of CO_2 at specific carbon sites, such as the carbonyl groups formed by oxidation pretreatment. One electron transfer to this site generates a ·C-O^- center, with the charge localized on the carbon activating the nearlying C-C bond making susceptible of activating the oxygen in the O=C bond of carbon dioxide, thus generating a δ+ charge on C of CO_2, facilitating the electron transfer from ·C-O^- center. In a different paper on the reactivity of carbon nanotubes (modified by a specific surface nitrogen doping mechanism), we showed that the amount of nitrogen in CNTs influences the performances in the electrocatalytic reduction of CO_2. The behaviour linearly correlated with the change of work function in these materials. The latter aspect influences the electronic coupling between electron donor/acceptor and in turn the rate of electron transfer.

This can provide an explanation of the role of metal nanoparticles in our electrocatalysts. It may be noted, in fact, that there are differences in the behaviour and productivity, but limited with respect to the very relevant change in the type of metal nanoparticles, from Pt to Cu, Fe and Co. If the reaction occurs only at the metal surface, much greater differences are expected. On the other hand, metal nanoparticles may change locally the work function of carbon, thus facilitating the electron transfer. It may be also facilitate the electron transfer to protons, generating H· species, which are more reactive in reacting with oxygen of CO_2 or with the products of its reduction. The metal will thus act as co-catalyst with the functional groups present on activated carbon, rather than as unique catalytic site. The sites will thus be mainly located at the perimetral edge between carbon and metal particles, in agreement with previous studies by calorimetry on this type of electrocatalysts for the reduction of CO_2 [49]. Although clearly further demonstrations are necessary to support this mechanism, it can provide preliminary indications on the aspects investigated, being different from the actual mechanisms proposed for CO_2 electrocatalytic conversion, which are focused only on the role of metal surface.

Reasonably the intermediate generated in this mechanism of reduction of CO_2 requires a solvent to be stabilized. On the other hand, metal nanoparticles are easy passivated, because CO_2 dissociation at the electrocatalyst metal surface generates CO and an O species, both remaining strongly bound to the metal surface. In the absence of the bulk electrolyte, both the absence of the solvent (electrolyte) and the higher CO_2 concentration at the surface of the electrocatalyst reasonably contribute in inhibiting on one side the mechanism of electron transfer/hydrogenation of CO_2 (via formic acid and formaldehyde), promoting on the other hand the mechanism of CO_2 dissociation to CO at the metal surface or reasonably at the metal-carbon perimetral region. The further reaction of adsorbed species on the metal surface leads to C-C bond formation and to the products observed experimentally.

Although speculative, this change of the type of mechanism of CO_2 reduction may explain the differences observed in both productivity, type of products and relative rates of reactions between different electrodes. These observation evidences how a more complex surface chemistry in the electrocatalytic reduction of CO_2 may exist with respect to what suggested in literature. A better understanding of these aspects opens new possibilities in controlling the type of products formed and their productivity, as evidenced from the comparison between liquid- and gas-phase operations on the same electrodes. On the other hand, the results also remark that carbon may be not only a support, but it plays a relevant role in understanding the chemistry of reduction of CO_2. This also opens new possibilities in the design of the electrocatalysts for the reduction of CO_2 and of the critical elements to consider for their improvement.

Conclusions

The comparison of the same electrodes for the electrocatalytic reduction of CO_2 in operations in the presence (liquid-phase) or absence (gas-phase) of a bulk electrolyte provide a series of interesting indications both on the limiting steps of the process and on the reaction mechanism.

It is demonstrated that under electrolyte-less (EL) operations, the productivity in the reduction of CO_2 is about one order of magnitude larger, and different type of products are formed. This is related to differences in the reaction mechanism, which were discussed, although further studies are needed to clarify better the reaction mechanism and the influence of the presence of the electrolyte.

In liquid-phase operations it is suggested that the mechanism involves the step reduction via intermediate formation of formic acid and formaldehyde and finally methanol, although the latter step is observed only in some electrodes. In fact, due to the strong acid conditions present at the electrocatalyst, located at the interface with Nafion membrane, formic acid decomposes to generate CO, which reacts with formaldehyde to form acetic acid. Methanol also reacts further in these strong acid conditions to form methyl formate.

In gas-phase operations, this mechanism is not longer effective and the conversion of CO_2 involves its dissociation to CO, which remains strongly chemisorbed, giving rise to further transformation reactions and formation of C-C bonds that produce a different spectrum of products of that observed in liquid-phase operations.

The electrocatalysts utilized here are based on metal nanoparticles (Fe, Cu, Co, Pt) deposited on two types of conductive carbon supports: carbon nanotubes functionalized by oxidation treatment (CNT_{ox}) and Vulcan XC-72 carbon black (CB). CNT_{ox} without metal particles is active both in producing H_2 from protons/electrons and in the reduction of CO_2. The possible mechanism and the role of carbonyl groups, formed during the oxidative treatment, is outlined. It is commented why in general also when metal nanoparticles are present, the carbon does not act only as support or to transport charges, but has also an active role in the reaction mechanism. It is suggested that the active sites for the electrocatalytic reduction of CO_2 are located at the perimetral edge between

metal nanoparticles and the carbon. The nature of the latter, in particular the type of surface functional groups, determine thus considerably the performances, as experimentally observed.

As commented, these results are the start, not the end of the analysis of the mechanism of reaction in the type of electrodes investigated here. However, we believe that these results evidence how a more complex surface chemistry than typically supposed in literature is present in the electrocatalytic reduction of CO_2 on the type of electrodes we investigated. It should be commented that their performances are better than that of various other electrodes reported in literature for the conversion of CO_2, even if the different reaction conditions and way to report the data do not often allow a precise comparison.

There is thus the need of a better understanding of the performances and reaction mechanism of these electrocatalysts (based on metal nanoparticles on conductive, functionalized carbon support) for the reduction of CO_2. They may open new possibilities in controlling the type of products formed and their productivity in this challenging reaction.

Acknowledgements

The authors acknowledge the PRIN10-11 projects "Mechanisms of activation of CO_2 for the design of new materials for energy and resource efficiency" and the EU project ECO^{2}CO$_2$ ("Eco-friendly biorefinery fine chemicals from CO_2 photocatalytic reduction"), which have partially supported this work. C. Marepally also thanks the European Doctoral Programme on Sustainable Industrial Chemistry (SINCHEM) for supporting his PhD programme.

Notes and references

1 G.A. Ozin, *Adv. Mat*., 2015, **27**, 1957.
2 G. Centi, S. Perathoner, in Green Carbon Dioxide, G. Centi, S. Perathoner, Eds., Wiley & Sons 2014, Ch. 1, 1.
3 M.D. Kaerkaes, O. Verho, E.V. Johnston, B. Aakermark, *Chem. Rev.,* 2014, **114**, 11863.
4 S. Protti, A. Albini, N. Serpone, *Phys. Chem. Chem. Phys*., 2014, **16**, 19790.
5 C. van der Giesen, R. Kleijn, G.J. Kramer, *Env. Science & Techn*., 2014, **48**, 7111.
6 J.M. Thomas, *Energy & Env. Science*, 2014, **7**, 19.
7 S. Bensaid, G. Centi, E. Garrone, S. Perathoner, G. Saracco, *ChemSusChem*, 2012, **5**, 50.
8 G. Centi, S. Perathoner, *Greenhouse Gases: Science and Techn*., 2011, **1**, 21.
9 G. Centi, S. Perathoner, *ChemSusChem*, 2010, **3**, 195.
10 D.G. Nocera, *Acc. Chem. Res*., 2012, **45**, 767.
11 C. Ampelli, S. Perathoner, G. Centi, *Phil. Trans. Royal Soc., A: Math., Phys. & Eng. Sciences*, 2015, **373**, 1.
12 P. Lanzafame, G. Centi, S. Perathoner, *Chem. Soc. Rev*., 2014, **43**, 7562.
13 S. Perathoner, G. Centi, *ChemSusChem*, 2014, **7**, 1274.
14 G. Centi, E.A. Quadrelli, S. Perathoner, *Energy & Envi. Science*, 2013, **6**, 1711.
15 S. Perathoner, G. Centi, *J. Chinese Chem. Soc*.. 2014, **61**, 719.
16 G. Centi, S. Perathoner, Artificial leaves, in *Kirk-Othmer Encyclopedia of Chemical Technology*, 2014.
17 J. Albo, M. Alvarez-Guerra, P. Castano, A. Irabien, *Green Chem*., 2015, **17**, 2304.
18 P. Kang, Z. Chen, M. Brookhart, T.J. Meyer, *Top. Catal*., 2015, **58**, 30.
19 Q. Lu, J. Rosen, F. Jiao, *ChemCatChem*, 2015, **7**, 38.
20 E.S. Rountree, B.D. McCarthy, T.T. Eisenhart, J.L. Dempsey, *Inorg. Chem*., 2014, **53**, 9983.
21 J. Qiao, Y. Liu, F. Hong, J. Zhang, *Chem. Soc. Rev*., 2014, **43**, 631.
22 E.V. Kondratenko, G. Mul, J. Baltrusaitis, G.O. Larrazabal, J. Perez-Ramirez, *Energy & Env. Science*, 2013, **6**, 3112.
23 C. Genovese, C. Ampelli, S. Perathoner, G. Centi, *J. Energy Chem*., 2013, **22**, 202.
24 G. Centi, S. Perathoner, in *Chemical Energy Storage*, R. Schlögl Ed., De Gruyter 2013, 379.
25 K.S. Joya, Y.F. Joya, K. Ocakoglu, R. van de Krol, *Angew. Chemie, Int. Ed.* 2013, **52**, 10426.
26 J. Barber, P.D. Tran, *J. Royal Soc. Interface*, 2013, **10**, 20120984.
27 M.D. Kaerkaes, O. Verho, E.V. Johnston, B. Aakermark, *Chem. Rev*., 2014, **114**, 11863.
28 S. Fukuzumi, Y. Yamada, *ChemSusChem*, 2013, **6**, 1834.
29 D.K. Bora, A. Braun, E.C. Constable, *Energy & Env. Science*, 2013, **6**, 407.
30 C. Ampelli, G. Centi, R. Passalacqua, S. Perathoner, *Catal. Today*, 2015, submitted.
31 C. Ampelli , C. Genovese, S. Perathoner, G. Centi, M. Errahali, G. Gatti, L. Marchese, *Chem. Eng. Trans*., 2014, **41**, 13; C. Ampelli, C. Genovese, R. Passalacqua, S. Perathoner, G. Centi. *Theor. Found. Chem. Eng*., 2012, **46**, 651.
32 C. Genovese, C. Ampelli, S. Perathoner, G. Centi, *J. Catal*., 2013, **308**, 237; C. Ampelli, S. Perathoner, G. Centi, *Chinese J. Catal*., 2014, **35**, 783.
33 C. Ampelli, G. Centi, R. Passalacqua, S. Perathoner, *Energy & Env. Science*, 2010, **3**, 292.
34 G. Centi, S. Perathoner, G. Wine, M. Gangeri, *Green Chem*., 2007, **9**, 671.
35 K.P. Kuhl, E.R. Cave, D.N. Abramc, T.F. Jaramillo, *Energy & Environ. Sci*., 2012, **5**, 7050.
36 P. Hirunsit, W. Soodsawang, J. Limtrakul, *J. Phys. Chem. C*, 2015, **119**, 8238.
37 Q. Shen, Z. Chen, X. Huang, M. Liu, G. Zhao, *Env. Science & Techn*., 2015, **49**, 5828-
38 J. Albo, M. Alvarez-Guerra, P. Castano, A. Irabien, *Green Chem*., 2015, **17**, 2304.
39 S. Back, H. Kim, Y. Jung, *ACS Catal*., 2015, **5**, 965.
40 S. Rasul, D.H. Anjum, A. Jedidi, Y. Minenkov, L. Cavallo, K. Takanabe, *Angew. Chemie, Int. Ed*., 2015, **54**, 2146.
41 C. Ampelli, C. Genovese, P. Lanzafame, S. Perathoner, G. Centi. *Chem. Eng. Trans*., 2014, **39**, 1627.
42 C. Ampelli, R. Passalacqua, C. Genovese, S. Perathoner, G. Centi, T. Montini, V. Gombac, P. Fornasiero. *Chem. Eng. Trans*., 2013, **35**, 583; C. Ampelli, R. Passalacqua, C. Genovese, S. Perathoner, G. Centi, T. Montini, V. Gombac, J.J. Delgado, P. Fornasiero, *RSC Advances*, 2013, **3**, 21776.
43 C. Ampelli, C. Genovese, R. Passalacqua, S. Perathoner and G. Centi, *Appl. Therm. Eng.*, 2014, **70**, 1270.
44 D.-W. Wang, D.S. Su, *Energy Environ. Sci*., 2014,**7**, 576.
45 G. Centi, S. Perathoner, D.S. Su, *Catal. Surveys from Asia*, 2014, **18**, 149; D.S. Su, S. Perathoner, G. Centi, *Chem. Rev*., 2013, **113** , 5782.
46 L. Kaplan, *J. Org. Chem*. 1985, **50**, 5376.
47 J.K. Nørskov, J. Rossmeisl, A. Logadottir, L. Lindqvist, J.R. Kitchin, T. Bligaard, H. Jónsson, *J. Phys. Chem. B*, 2004, **108**, 17886.
48 J. Xu, R. Huang, X. Sun, B. Zhang, Y.Lin,Q. Li, D. Su, G. Centi, *ACS Catalysis*, 2015, submitted.

49 R. Arrigo, M.E. Schuster, S. Wrabetz, F. Girgsdies, J.-P. Tessonnier, G. Centi, S. Perathoner, D.S. Su, R. Schlögl, *ChemSusChem*, 2012, **5**, 577.